Blind estimation of modulation parameters for PCMA signals using frame cyclic features

Fang Li[1][*] , Zhaoyang Qiu[1], Xiong Zha[1] and Tianyun Li[1]

*Correspondence:
franklee_2021@163.com

[1] Institute of Information System Engineering, Information Engineering University, Zhengzhou, China

Abstract

Blind receiver technologies for paired carrier multiple access (PCMA) signals have always been a challenging task with many technical difficulties, among which the estimation of modulation parameters is a fundamental but important element. Despite some achievements in previous studies, more systematic and sophisticated estimation methods have not been adequately investigated. In this paper, schemes for the blind estimation of the symbol timing phase, amplitude attenuation, frequency offset, and carrier phase for PCMA signals in satellite communications are proposed. The data flow transmitted in satellite communication often has a certain frame structure, the most important of which is the synchronization data, namely the so-called cycle features. The proposed schemes assume that the modulated signals have fixed frame length and frame sync code and that the symbol rate has been estimated when the signals are encoded asynchronously. Distinct from the previous methods, our schemes exploit the sync waveform and the overlapping waveform, which are estimated via singular value decomposition (SVD) (using the frame cyclic features) and interference cancelation, together with their demodulation results as aid data, for the estimation of the desired parameters. The simulation results demonstrate that the schemes are effective in the parameters estimation of PCMA signals and outperform the comparison algorithms.

Keywords: PCMA, Blind receiver, SVD, Frame cyclic features, Parameters estimation

1 Introduction

Paired carrier multiple access (PCMA) is a frequency-domain multiplexing multiple access technology for satellite communication proposed by ViaSat [1]. In the PCMA system, the satellite transponder retransmits its received uplink signals from the ground stations, assigning them to a common time–frequency resource in the downlink without any demodulation or reconstruction, in another word, the ground station would receive the mixture of local signal (self-interference signal) and far-end signal (useful signal) at the same frequency. In contrast to any other communications, it relies on self-interference cancelation (SIC) to separate the signals from different base stations. The SIC process involves subtracting the own transmitted signal from the received signals so that the far-end signals from the other base stations can be extracted. This makes PCMA an attractive option for satellite communications, as it allows two users to share a common

Li *et al. EURASIP Journal on Advances in Signal Processing*   (2023) 2023:95

Page 2 of 18

time–frequency resource, thereby improving the frequency band utilization. However, a third receiver may acquire the downlink signal without any prior knowledge; in other words, the reception is "blind."

Various separation approaches have been proposed to perform joint demodulation of the two overlapping signals [2–7]. With the development of deep learning, back propagation (BP) neural network and other deep learning models have been applied to the blind separation of PCMA signals [8]. Nevertheless, such approaches necessitate a familiarity with the channel and signal parameters, of which the estimation schemes are worth exploring.

The most common method to estimate the PCMA signal and channel parameters is based on cyclic statistics [9–11] and the maximum-likelihood (ML) criterion [12]. The cyclic statistics-based methods could be applied to most types of PCMA signals. However, owing to terrific amounts of cross terms emerging after M-power operation in high-order modulated PCMA signals such as 8 phase-shift keying (8PSK), the frequency offset estimation (FOE) algorithm is rendered inapplicable. Fortunately, the data-aided (DA) ML algorithm in [12] was able to successfully address the FOE issue associated with 8PSK-modulated PCMA signals, which can be also applied to low-order modulated PCMA signals. However, sync code is required to make the algorithm work, while it is not available in the totally blind scenario. In this case, the frame structure features of the signals can be used to obtain the method to solve the problem. Because of the cyclic characteristics of the frame synchronization data, it is possible to be estimated. In this paper, an approach is given to obtain the sync waveform using the singular value decomposition (SVD) method which is a popular technology for multi-channel signal processing [13]. Then, the waveform overlapping with the sync waveform is recovered via interference cancelation. Symbol timing phase is estimated by modified O &M algorithm [14]. Furthermore, as the waveforms demodulated, amplitude attenuation, frequency offset, and carrier phase could be estimated, using the demodulation results as aid data. Hence, parameters estimation of the PCMA signal under the condition of totally blind reception is realized.

Compared to the existing DA methods, our scheme solved the problem of aid data estimation and the utilization of overlapping waveform boosts the accuracy. The advantage compared to the cyclic statistics-based algorithms is that the introduction of aid data makes the algorithm more reliable and robust. Therefore, the scheme proposed in this paper has made significant progress in the parameters estimation of PCMA signals and outperforms the comparison algorithms.

In this paper, it is assumed that the modulated signals have a fixed frame length and frame sync code, provided that the signals have been encoded asynchronously. As we all know, frame synchronization is a common technology which is widely employed in satellite communications. In other words, it is reasonable to assume that most of the satellite signals might be designed with frame structure and sync codes. In addition, the sync codes are relatively shorter compared to the information codes and two signals are emitted by the ground stations independently. So, the signals are encoded asynchronously in high probability. Moreover, it is assumed that the channel is slowly time-varying, meaning that its parameters remain constant during the observed signal segments of the suitable size. In view of the wide application of amplitude and phase modulation (APM) in

PCMA systems (e.g., BPSK, QPSK, 8PSK, 8QAM, 16QAM, etc.), APM-modulated signals are assumed. The symbol rate can be estimated based on cyclic statistics [9], so the symbol rate is assumed as a known condition.

The rest of this paper is organized as follows. Section 2 presents the signal model and some significant assumptions. Section 3 introduces the sync waveform and overlapping waveform estimation method. Sections 4 and 5 propose estimation algorithms for the symbol timing phase, amplitude attenuation, frequency offset, and carrier phase. Section 6 presents the method of overlapping waveform demodulation. Complexity analysis of the proposed method is offered in Sect. 7. Section 8 provides the simulation results, demonstrating the effectiveness of the proposed schemes. Finally, Sect. 9 presents the conclusions.

2 Signal model

In the equivalent complex baseband domain, the received mixture of two adjacent-frequency APM-modulated signals can be expressed as

$$y(t) = h_1 e^{j(\omega_1 t + \theta_1)} x_1(t) + h_2 e^{j(\omega_2 t + \theta_2)} x_2(t) + v(t) \tag{1}$$

where h_i, ω_i, and θ_i are the amplitude attenuations, residual frequency offsets, and initial phases of the two APM signals, respectively. $v(t)$ denotes complex additive white Gaussian noise (AWGN) with zero mean and variance of σ_v^2, and $x_i(t)$ are defined as

$$x_i(t) = \sum_{n=-\infty}^{+\infty} s_i(n) g_i(t - nT - \tau_i) \tag{2}$$

where $s_i(n)$ are equiprobable, independent, and identically distributed (i.i.d.) random sequences with unit energy, transmitted by the two APM signals, $g_i(t)$ are the pulse responses of the equivalent channel filters, T is the symbol period, and τ_i are the symbol timing phases with an interval of $[0, T)$.

Sampling the signal at period $T_s = T/p$, where p is the up-sample times and an integer, the durations of the equivalent channel filters are assumed as $[-L_1 T, L_2 T]$, and the resulting discrete-time signal can be written as

$$y_k(l) = \sum_{i=1}^{2} \left[h_i e^{j[\omega_i(k + l/p)T + \theta_i]} \sum_{m=-L_1}^{L_2} s_i(k+m) g_i(-mT + lT/p - \tau_i) \right] + v_k(l) \tag{3}$$

where $k = 0, 1, 2, \ldots$ represents the indices of symbols, $l = 0, 1, \ldots, p-1$, $y_k(l) = y[(k + l/p)T]$, $v_k(l) = v[(k + l/p)T]$. With $L = L_1 + L_2 + 1$, we can define $L \times 1$ equivalent channel response vector as follows:

$$\mathbf{g}_{i,l} = [g_i(L_1 T + lT/p - \tau_i), \ldots, g_i(-L_2 T + lT/p - \tau_i)]^{\mathrm{T}} \tag{4}$$

The input symbol vectors during the *k*th symbols are denoted as

$$\mathbf{s}_{i,k} = [s_i(k - L_1), \ldots, s_i(k + L_2)]^{\mathrm{T}} \tag{5}$$

$y_k(l)$ can be rewritten as

$$y_k(l) = \sum_{i=1}^{2} h_i \mathbf{g}_{i,l}^{\mathrm{T}} \mathbf{s}_{i,k} e^{j[\omega_i(k+l/p)T + \theta_i]} + v_k(l) = \bar{y}_k(l) + v_k(l) \tag{6}$$

$\bar{y}_k(l)$ represent the useful signals.

Sampling the signal at symbol period T, the discrete-time signal can be written as

$$y_T(k) = \sum_{i=1}^{2} h_i e^{j(\omega_i kT + \theta_i)} x_T^{(i)}(k) + v_T(k) \tag{7}$$

$x_T^{(i)}(k)$ and $v_T(k)$ satisfy

$$\begin{cases} x_T^{(i)}(k) = \sum\limits_{m=-L_1}^{L_2} s_i(k+m) g_i(-mT - \tau_i) \\ v_T(k) = v(kT) \end{cases} \tag{8}$$

3 Sync waveform and overlapping waveform estimation

Representatively, we could assume that the two overlapping signals possess the same frame length N_s and an asynchronous coding structure, meaning that their sync codes do not overlap. As shown in Fig. 1, each frame signal contains H sync code symbols, and upon the segment of the processed signal, the sync code symbols start at o_1 and o_2, respectively.

Taking the oversampling PCMA mixed signal sample $y_k(l)$ with length N_r, and assuming N_r is large enough, the estimation of the signal autocorrelation function $R_y(k)$ could be expressed as

$$\begin{aligned} \widehat{R}_y(k) &= \widehat{R}_y(pk_1 + l_1 - pk_2 - l_2) \\ &= \frac{1}{N_r} \sum_{n=1}^{N_r-1} y_{k_1}(l_1) y_{k_2}{}^*(l_2) \\ &= \frac{1}{N_r} \sum_{n=1}^{N_r-1} [\bar{y}_{k_1}(l_1) + v_{k_1}(l_1)][\bar{y}_{k_2}(l_2) + v_{k_2}(l_2)]^* \\ &\approx \frac{1}{N_r} \sum_{n=1}^{N_r-1} \bar{y}_{k_1}(l_1) \bar{y}_{k_2}(l_2)^* \end{aligned} \tag{9}$$
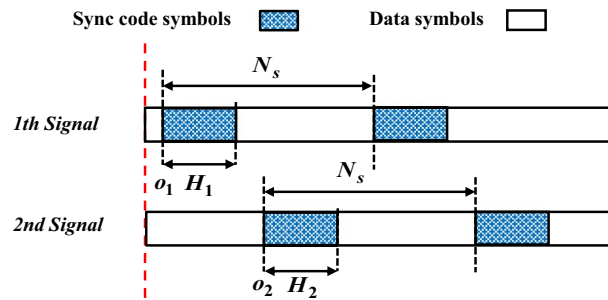

Fig. 1 Scheme of asynchronous coding in two signals

where $k = 0, 1, \ldots, K_r, 1 \ll K_r < N_r$. Substituting Eq. (6) into Eq. (9), considering that the elements in vector $\mathbf{s}_{i,k}$ obey the uniform distribution with zero mean and the two APM signals are uncorrelated, the following equation can be derived

$$
\begin{aligned}
\widehat{R}_y(k) &= \widehat{R}_y(pk_1 + l_1 - pk_2 - l_2) \\
&\approx \frac{1}{N_r} \sum_{i=1}^{2} \sum_{n=1}^{N_r-1} h_i^2 (\mathbf{g}_{i,l_1}^{\mathrm{T}} \mathbf{s}_{i,k_1})(\mathbf{g}_{i,l_2}^{\mathrm{T}} \mathbf{s}_{i,k_2})^* e^{j\omega_i k T_s}
\end{aligned}
\tag{10}
$$

Assume that the frame numbers of the two APM signals contained in the PCMA signal are far greater than 1. It can be observed in Eq. (10) that if $\mathbf{g}_{1,l_1}^{\mathrm{T}} \mathbf{s}_{1,k_1}$ and $\mathbf{g}_{1,l_2}^{\mathrm{T}} \mathbf{s}_{1,k_2}$, $\mathbf{g}_{2,l_1}^{\mathrm{T}} \mathbf{s}_{2,k_1}$, and $\mathbf{g}_{2,l_2}^{\mathrm{T}} \mathbf{s}_{2,k_2}$ are not correlated with each other, then $\widehat{R}_y(k) = 0$, if $\mathbf{g}_{1,l_1}^{\mathrm{T}} \mathbf{s}_{1,k_1}$ and $\mathbf{g}_{1,l_2}^{\mathrm{T}} \mathbf{s}_{1,k_2}$, or $\mathbf{g}_{2,l_1}^{\mathrm{T}} \mathbf{s}_{2,k_1}$ and $\mathbf{g}_{2,l_2}^{\mathrm{T}} \mathbf{s}_{2,k_2}$ are correlated with each other, then $\widehat{R}_y(k) \neq 0$, and the stronger the correlation, the greater the value of $\widehat{R}_y(k)$. When k aligning the first signal synchronization symbol or the second signal synchronization symbol, the relevance reaches a maximum, the peak of $\widehat{R}_y(k)$ occurs. Assuming that both the symbol rates of the two APM signals are R_B, the peak of $\widehat{R}_y(k)$ would occur at $k_{\max} = pN_s$ and its integral multiple position. Therefore, by searching the peaks of $\widehat{R}_y(k)$, we can obtain the estimation of symbol frame length

$$
\hat{N}_s = [k_{\max}/p]
\tag{11}
$$

where $[\cdot]$ presents rounding.

With frame length estimated, the oversampled signal is segmented with frame length $N = pN_s$ to obtain data matrix $\mathbf{A}$.

When $(\omega_1 - \omega_2)NT_s = 2m\pi$, it can be proven that the autocorrelation matrix can be expressed as

$$
\widehat{\mathbf{R}}(P) = \frac{1}{P} \mathbf{A}\mathbf{A}^{\mathrm{H}} = (\mathbf{b}_1 + \mathbf{b}_2)(\mathbf{b}_1 + \mathbf{b}_2)^{\mathrm{H}} + \mathbf{\Lambda} + \sigma_v^2 \mathbf{I}
\tag{12}
$$

When $(\omega_1 - \omega_2)NT_s \neq 2m\pi$, the autocorrelation matrix can be expressed as

$$
\widehat{\mathbf{R}}(P) = \frac{1}{P} \mathbf{A}\mathbf{A}^{\mathrm{H}} = \mathbf{b}_1 \mathbf{b}_1^{\mathrm{H}} + \mathbf{b}_2 \mathbf{b}_2^{\mathrm{H}} + \mathbf{\Lambda} + \sigma_v^2 \mathbf{I}
\tag{13}
$$

P is the number of signal frames. $\mathbf{\Lambda}$ is a diagonal matrix, $\mathbf{I}$ is an identity matrix, and

$$
\mathbf{b}_1 = \begin{bmatrix} \mathbf{0} \\ h_1 \mathbf{g}_{1,0}^{\mathrm{T}} \mathbf{s}_{1,r_1^{(1)}} e^{j[\omega_1 pr_1^{(1)} T_s + \varphi_1]} \\ \vdots \\ h_1 \mathbf{g}_{1,p-1}^{\mathrm{T}} \mathbf{s}_{1,r_2^{(1)}} e^{j[\omega_1 (pr_2^{(1)} + p - 1)T_s + \varphi_1]} \\ \mathbf{0} \end{bmatrix}, \mathbf{b}_2 = \begin{bmatrix} \mathbf{0} \\ h_2 \mathbf{g}_{2,0}^{\mathrm{T}} \mathbf{s}_{2,r_1^{(2)}} e^{j[\omega_2 pr_1^{(2)} T_s + \varphi_2]} \\ \vdots \\ h_2 \mathbf{g}_{2,p-1}^{\mathrm{T}} \mathbf{s}_{2,r_2^{(2)}} e^{j[\omega_2 (pr_2^{(2)} + p - 1)T_s + \varphi_2]} \\ \mathbf{0} \end{bmatrix}
\tag{14}
$$

$[r_1^{(i)}, r_2^{(i)}]$ is the sync code interval of the ith signal, and $\varphi_1 - \varphi_2 = \theta_1 - \theta_2$. Obviously, with $\mathbf{b}_1$, $\mathbf{b}_2$ obtained, we can get the sync waveform estimation of the dual signals.

When $(\omega_1 - \omega_2)NT_s = 2m\pi$, we can approximately expect that

$$(\mathbf{b}_1 + \mathbf{b}_2) \approx \sqrt{\lambda_1}\mathbf{u}_1 \tag{15}$$

When $(\omega_1 - \omega_2)NT_s \neq 2m\pi$, the sync waveform energies of two signals are unequal

$$\mathbf{b}_1 \approx \sqrt{\lambda_1}\mathbf{u}_1, \mathbf{b}_2 \approx \sqrt{\lambda_2}\mathbf{u}_2 \tag{16}$$

When $(\omega_1 - \omega_2)NT_s \neq 2m\pi$, the sync waveform energies of two signals are equal

$$\begin{cases} \sqrt{\lambda_1}\mathbf{u}_1 \approx x_1\mathbf{b}_1 + x_2\mathbf{b}_2 \\ \sqrt{\lambda_2}\mathbf{u}_2 \approx y_1\mathbf{b}_1 + y_2\mathbf{b}_2 \end{cases} \tag{17}$$

where x_1, x_2, y_1, y_2 satisfies $x_1^2 = y_2^2 = \rho_1^2$, $x_2^2 = y_1^2 = \rho_2^2$, $x_1x_2 = -y_1y_2$, $\rho_1^2 + \rho_2^2 = 1$, $\rho_1, \rho_2 > 0$. λ_i, $\mathbf{u}_i$ are the ith eigenvalue and eigenvector of $\widehat{\mathbf{R}}(P)$.

Hence, the estimation of the ith signal's sync waveform is obtained

$$z_{i,k}(l) = h_i'\mathbf{g}_{i,l}^{\mathrm{T}}\mathbf{s}_{i,k}e^{j[\omega_i(pk+l)T_s+\varphi_i]} + v_{i,k}(l) \tag{18}$$

where $k \in [r_1^{(i)}, r_2^{(i)}]$, $l = 0, \ldots, p-1$, $h_i' = h_i$ except the situation of Eq. (17), in which the sync waveform estimation can be obtained by taking any pair of eigenvalue and eigenvector temporarily, and its amplitude will be further adjusted in the subsequent processing. $v_{i,k}(l)$ is the equivalent AWGN with zero mean and variance σ_i^2.

The nth frame waveform of the PCMA signal can be written as

$$\begin{aligned} y_k^n(l) &= h_1\mathbf{g}_{1,l}^{\mathrm{T}}\mathbf{s}_{1,nN_s+k}e^{j[\omega_1(nN+pk+l)T_s+\theta_1]} \\ &\quad + h_2\mathbf{g}_{2,l}^{\mathrm{T}}\mathbf{s}_{2,nN_s+k}e^{j[\omega_2(nN+pk+l)T_s+\theta_2]} + v_{nN_s+k}(l) \end{aligned} \tag{19}$$

where $k \in [0, N_s - 1]$. Define the correlation between $z_{i,k}(l)$ and $y_k^n(l)$ as

$$\begin{aligned} R_{nN}^{(i)} &= \frac{1}{N_i}\sum_{k=r_1^{(i)}}^{r_2^{(i)}}\sum_{l=0}^{p-1}y_k^n(l)[z_{i,k}(l)]^* \\ &\approx \frac{1}{N_i}\sum_{k=r_1^{(i)}}^{r_2^{(i)}}\sum_{l=0}^{p-1}h_ih_i'\left|\mathbf{g}_{i,l}^{\mathrm{T}}\mathbf{s}_{i,k}\right|^2 e^{j(\omega_i(n-1)NT_s+\theta_i-\varphi_i)} \end{aligned} \tag{20}$$

Then, we can get the nth frame sync waveform with phase corrected

$$z_{i,k}^n(l) = e^{j\cdot\mathrm{angle}\{R_{nN}^{(i)}\}} \cdot z_{i,k}(l) \tag{21}$$

After detection and extraction, the sync waveform is rewritten as $x_i^n(\kappa)$, $\kappa = p(nN_s + k) + l$, $\kappa \in [\kappa_1^{(i)}, \kappa_2^{(i)}]$, and $[\kappa_1^{(i)}, \kappa_2^{(i)}]$ is the interval of the sync waveform.

The sync waveform estimation procedure is shown in Fig. 2. First of all, autocorrelation is calculated to estimate the frame length N_s. And then, the signal is segmented by frame length $N = pN_s$ to obtain data matrix $\mathbf{A}$ and SVD processing is adopted. The eigenvectors corresponding to the two maximum eigenvalues are displayed in Fig. 2. The three graphs represent the situations in Eqs. (15), (16), and (17), respectively. The envelope with higher energy indicates the location where the sync waveform exists.
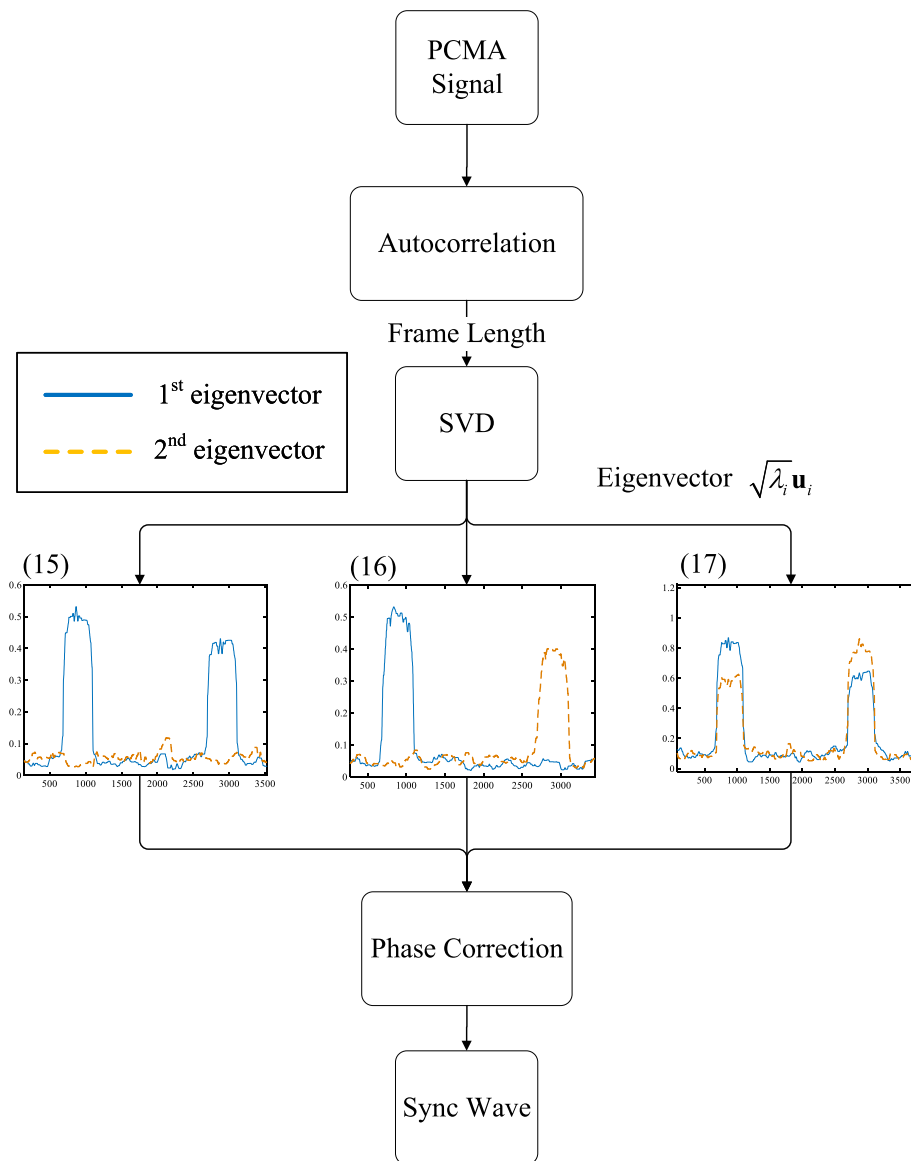
Fig. 2 Diagram of the sync waveform estimation

We could estimate the sync waveform according to the SVD results. Finally, the phase of the waveform is corrected, and the desired sync waveform is obtained.

Once the sync waveform estimated, the overlapping waveform in the sync interval could be obtained by subtracting the sync waveform estimated.

4 Symbol timing phase and amplitude attenuation estimation

With the sync waveform $x_i^n(\kappa)$ estimated, the O &M algorithm can be modified to get the symbol timing phase of the two signals

$$\hat{\tau}_i = -\frac{T}{2\pi}\text{angle}\left\{\sum_{n=0}^{P-1}\sum_{\kappa=\kappa_1^{(i)}}^{\kappa_2^{(i)}}\left|x_i^n(\kappa)\right|^2 e^{-j2\pi\kappa/p}\right\} \tag{22}$$

Then, the optimal sampling sequence of $x_i^n(\kappa)$ can be written as $x_{i,T}^n(k)$, $k = 1, 2, \ldots, H$. After timing synchronization, owing to the length of sync code that will not be long, the sync waveform could be demodulated despite residual frequency offset, and we can get the sync code estimation $\alpha_i(k)$. Thereupon, the amplitude attenuation estimation of $x_i^n(\kappa)$ can be obtained by utilizing the estimated sync code and the optimal sampling sequence, where the sync code could be regarded as aid data

$$\hat{h}_i' = \frac{1}{PH}\sum_{n=0}^{P-1}\sum_{k=1}^{H}\frac{\left|x_{i,T}^n(k)\right|}{\left|\alpha_i(k)\right|} \tag{23}$$

Subsequently, sync waveform with real amplitude attenuation is obtained in any case and is denoted as $\bar{x}_i^n(\kappa)$, and the waveform mixed with $\bar{x}_i^n(\kappa)$ can be obtained via

$$\tilde{x}_i^n(\kappa) = y_k(l) - \bar{x}_j^n(\kappa), i = \begin{cases} 1, & j = 2 \\ 2, & j = 1 \end{cases} \tag{24}$$

And then, the O &M algorithm can be revised as

$$\begin{cases} \hat{\tau}_1 = -\frac{T}{2\pi}\text{angle}\{\sum_{n=0}^{P-1}(\sum_{\kappa=\kappa_1^{(1)}}^{\kappa_2^{(1)}}\left|\tilde{x}_1^n(\kappa)\right|^2 e^{-j2\pi\kappa/p} + \sum_{\kappa=\kappa_1^{(2)}}^{\kappa_2^{(2)}}\left|\tilde{x}_2^n(\kappa)\right|^2 e^{-j2\pi\kappa/p})\} \\ \hat{\tau}_2 = -\frac{T}{2\pi}\text{angle}\{\sum_{n=0}^{P-1}(\sum_{\kappa=\kappa_1^{(1)}}^{\kappa_2^{(1)}}\left|\tilde{x}_1^n(\kappa)\right|^2 e^{-j2\pi\kappa/p} + \sum_{\kappa=\kappa_1^{(2)}}^{\kappa_2^{(2)}}\left|\bar{x}_2^n(\kappa)\right|^2 e^{-j2\pi\kappa/p})\} \end{cases} \tag{25}$$

5 FOE and carrier phase estimation

P frames are considered, $\boldsymbol{\Phi}_i = \{h_i, \tau_i, \omega_i, \theta_i\}$, $\bar{\mathbf{x}}_T^{(i)} = \{\bar{x}_{i,T}^n(k)\}$, $\tilde{\mathbf{x}}_T^{(i)} = \{\tilde{x}_{i,T}^n(k)\}$, $k = 1, \ldots, H$, $n = 0, \ldots, P-1$. $\bar{x}_{i,T}^n(k)$ is the optimal sampling sequence of $\bar{x}_i^n(\kappa)$, and $\tilde{x}_{i,T}^n(k)$ is the optimal sampling sequence of $\tilde{x}_i^n(\kappa)$. $X_T^{(i)} = \left\{\bar{\mathbf{x}}_T^{(i)}, \tilde{\mathbf{x}}_T^{(i)}\right\}$. When $i = 1$, the ML function can be written as

$$
\begin{aligned}
&p\left(X_T^{(1)}\Big|\Phi_1\right) \\
&= C_1 \cdot \exp\left[-\frac{1}{2\sigma_1^2}\sum_{n=0}^{P-1}\sum_{k=1}^{H}\left|\bar{x}_{1,T}^n(k) - h_1 e^{j[\omega_1(nN_s+o_1+k-1)+\theta_1]T}x_T^{(1)}(nN_s+o_1+k-1)\right|^2\right.\\
&\quad \left. -\frac{1}{2\tilde{\sigma}_1^2}\sum_{n=0}^{P-1}\sum_{k=1}^{H}\left|\tilde{x}_{1,T}^n(k) - h_1 e^{j[\omega_1(nN_s+o_2+k-1)T+\theta_1]}x_T^{(1)}(nN_s+o_2+k-1)\right|^2\right]\\
&= C_1 \cdot \exp\left[-\frac{1}{2\sigma_1^2}\sum_{n=0}^{P-1}\sum_{k=1}^{H}\left|e^{-j\omega_1(nN_s+o_1+k-1)T}\bar{x}_{1,T}^n(k) - h_1 e^{j\theta_1}x_T^{(1)}(nN_s+o_1+k-1)\right|^2\right.\\
&\quad \left. -\frac{1}{2\tilde{\sigma}_1^2}\sum_{n=0}^{P-1}\sum_{k=1}^{H}\left|e^{-j\omega_1(nN_s+o_2+k-1)T}\tilde{x}_{1,T}^n(k) - h_1 e^{j\theta_1}x_T^{(1)}(nN_s+o_2+k-1)\right|^2\right]
\end{aligned}
$$
$$\tag{26}$$

where $C_1 = (1/2\pi\sigma_1\tilde{\sigma}_1)^{H \cdot P}$, and $\tilde{\sigma}_i$ is the variance of the equivalent AWGN contained in overlapping waveform $\bar{x}_i^n(\kappa)$.

Because $x_T^{(i)}(k)$ is the optimal sampling sequence, we can obtain the relationship, $x_T^{(i)}(k) \approx s_i(k)$, $p(X_T^{(1)}|\mathbf{\Phi}_1)$ can be simplified as

$$p(X_T^{(1)}|\mathbf{\Phi}_1) \simeq C_1 \cdot \exp\left[-\frac{1}{2\sigma_1^2}\sum_{n=0}^{P-1}\sum_{k=1}^{H}\left|e^{-j\omega_1(nN_s+o_1+k-1)T}\bar{x}_{1,T}^n(k) - h_1 e^{j\theta_1}\alpha_1(k)\right|^2\right.$$
$$\left. -\frac{1}{2\tilde{\sigma}_1^2}\sum_{n=0}^{P-1}\sum_{k=1}^{H}\left|e^{-j\omega_1(nN_s+o_2+k-1)T}\tilde{x}_{1,T}^n(k) - h_1 e^{j\theta_1}\beta_1^n(k)\right|^2\right]$$

(27)

where $\alpha_i(k)$ is the sync code and $\beta_i^n(k)$ is the demodulation result of $\tilde{x}_i^n(\kappa)$.

By defining

$$\Omega_1(\mathbf{\Phi}_1) = \frac{1}{2\sigma_1^2}\sum_{n=0}^{P-1}\sum_{k=1}^{H}\left|e^{-j\omega_1(nN_s+o_1+k-1)T}\bar{x}_{1,T}^n(k) - h_1 e^{j\theta_1}\alpha_1(k)\right|^2$$
$$+\frac{1}{2\tilde{\sigma}_1^2}\sum_{n=0}^{P-1}\sum_{k=1}^{H}\left|e^{-j\omega_1(nN_s+o_2+k-1)T}\tilde{x}_{1,T}^n(k) - h_1 e^{j\theta_1}\beta_1^n(k)\right|^2$$

(28)

the maximization of $p(X_T^{(1)}|\mathbf{\Phi}_1)$ is equal to the minimization of $\Omega_1(\mathbf{\Phi}_1)$. Likewise, for $i = 2$, we obtain

$$\Omega_2(\mathbf{\Phi}_2) = \frac{1}{2\sigma_2^2}\sum_{n=0}^{P-1}\sum_{k=1}^{H}\left|e^{-j\omega_2(nN_s+o_2+k-1)T}\bar{x}_{2,T}^n(k) - h_2 e^{j\theta_1}\alpha_2(k)\right|^2$$
$$+\frac{1}{2\tilde{\sigma}_2^2}\sum_{n=0}^{P-1}\sum_{k=1}^{H}\left|e^{-j\omega_2(nN_s+o_1+k-1)T}\tilde{x}_{2,T}^n(k) - h_2 e^{j\theta_2}\beta_2^n(k)\right|^2$$

(29)

Obviously, it is impractical to accurately ascertain the value of ω_i by directly deriving (28) and (29). However, on condition that ω_i is accurately estimated, each term in $\Omega_i(\mathbf{\Phi}_i)$ will be approximately equal to zero. Thus, in the estimation of ω_i, the maximization of the cross-correlation computation and the minimization of the error computation between each term in $\Omega_i(\mathbf{\Phi}_i)$ are equivalent. Therefore, we can refine the ML function as

$$\begin{cases} \rho_1(\omega) = \left|\sum_{n=0}^{P-1}\sum_{k=1}^{H}\left(e^{-j\omega(nN_s+o_1+k-1)T}\bar{x}_{1,T}^n(k) \cdot [\alpha_1(k)]^* \right.\right. \\ \qquad\qquad \left.\left. +e^{-j\omega(nN_s+o_2+k-1)T}\tilde{x}_{1,T}^n(k) \cdot [\beta_1^n(k)]^*\right)\right| \\ \rho_2(\omega) = \left|\sum_{n=0}^{P-1}\sum_{k=1}^{H}\left(e^{-j\omega(nN_s+o_2+k-1)T}\bar{x}_{2,T}^n(k) \cdot [\alpha_2(k)]^* \right.\right. \\ \qquad\qquad \left.\left. +e^{-j\omega(nN_s+o_1+k-1)T}\tilde{x}_{2,T}^n(k) \cdot [\beta_2^n(k)]^*\right)\right| \end{cases}$$

(30)

While maximizing $\rho_i(\omega)$, the optimum value of ω_i would be determined, and FOE based on ML is completed. To ascertain the optimum value of ω_i, a hierarchical search method [12], with a low computational complexity, is an alternative approach.

The range of FOE will be limited if $\rho_i(\omega)$ has another maximum besides ω_i. There is no harm in assuming that there is another value, $\omega_i' = \omega_i + \Delta\omega_i$ can maximize $\rho_i(\omega)$ besides true value ω_i, $\Delta\omega_i$ satisfies $\Delta\omega_i(nN_s + o_t + k - 1)T = 2\,m\pi\,(m = 1, 2, \ldots; t = 1, 2)$. The maximum value of $\rho_i(\omega)$ will remain as long as $\Delta\omega_i$ satisfies the criteria of $\Delta\omega_i nN_s T = 2\,m\pi\,(m = 1, 2, \ldots)$, that is, $\Delta\omega_i = 2\,m\pi/N_s T$, while the term $e^{-j\Delta\omega_i(o_t+k-1)T}$ only has a slight effect on $\rho_i(\omega)$. The effective range of FOE can be derived as

$$|\omega| \leq \pi/N_s T \tag{31}$$

The FOE algorithm presented in this paper is an improvement of the one proposed in [12]. The difference lies in the fact that we obtain the synchronous waveform and overlapping waveform and demodulate them for the sync code and the overlapping code, utilizing all the sync information as aid data, whereas [12] only uses the sync code as aid data, assuming it as the prior information. As such, the algorithm proposed in this paper is anticipated to attain more favorable results.

Given frequency offsets are accurately estimated, the carrier phases can be derived via a data-aided method

$$\begin{cases} \hat{\theta}_1 = \text{angle}\left\{\sum_{n=0}^{P-1}\sum_{k=1}^{H}\left(e^{-j\omega_1(nN_s+o_1+k-1)T}\bar{x}_{1,T}^n(k)\cdot[\alpha_1(k)]^* \right.\right. \\ \qquad\qquad\qquad\left.\left. +e^{-j\omega_1(nN_s+o_2+k-1)T}\tilde{x}_{1,T}^n(k)\cdot[\beta_1^n(k)]^*\right)\right\} \\ \hat{\theta}_2 = \text{angle}\left\{\sum_{n=0}^{P-1}\sum_{k=1}^{H}\left(e^{-j\omega_2(nN_s+o_2+k-1)T}\bar{x}_{2,T}^n(k)\cdot[\alpha_2(k)]^* \right.\right. \\ \qquad\qquad\qquad\left.\left. +e^{-j\omega_2(nN_s+o_1+k-1)T}\tilde{x}_{2,T}^n(k)\cdot[\beta_2^n(k)]^*\right)\right\} \end{cases} \tag{32}$$

6 Sync waveform and overlapping waveform demodulation

When demodulating the overlapping waveform $\tilde{x}_i^n(\kappa)$, the initial phase of each piece of waveform is required to be estimated. Since the residual frequency offset may be large, the initial phase estimation algorithm is as follows [15]:

$$\hat{\phi}_i^n = \frac{1}{M}\text{angle}\left\{\sum_{k=1}^{H}e^{jM\arg[\tilde{x}_{i,T}^n(k)]}\right\} \tag{33}$$

The initial phase of each piece of sync waveform can be obtained by the initial phase of $z_{i,k}(l)$. Assume that the initial phase estimation of $z_{i,k}(l)$ is $\hat{\varphi}_i$, and then, the initial phase of $\bar{x}_i^n(\kappa)$ can be expressed as

$$\psi_i^n = \text{angle}\{R_{nN}^{(i)}\} + \hat{\varphi}_i \tag{34}$$

Due to the phase ambiguity in the initial phase estimation result, the residual phase in the demodulation results of each waveform segment is different. Consequently, the demodulation result is different from the real code or the real code with consistent phase offset which can be eliminated by operation.
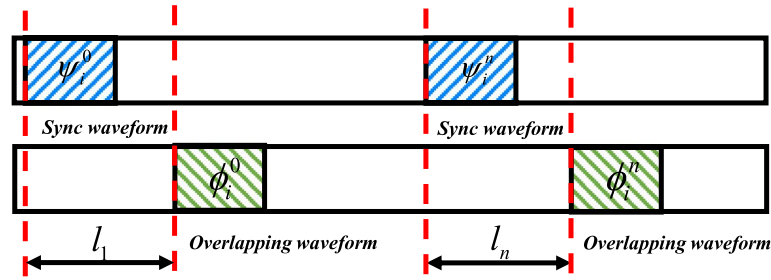
Fig. 3 Scheme of the initial phases of sync waveform and overlapping waveform

In order to make the FOE algorithm work, the effect of phase ambiguity during demodulation must be eliminated. As shown in Fig. 3, assuming the initial phase of the first overlapping waveform ϕ_i^0 and the initial phase of the sync waveform ψ_i^n are real, the following relationship can be obtained

$$\phi_i^0 - \psi_i^0 = \phi_i^n - \psi_i^n + m\pi/M \tag{35}$$

where $m = 0, \pm 1, \ldots, \pm(M-1)$. That is, due to the fixed position of synchronization sequence, more specifically $l_1 = l_n$, the initial phase differences between the adjacent sync waveforms and overlapping waveforms are equal. It is worth noting that there could be phase ambiguity in the estimation of ϕ_i^0 as well. To eliminate the effect of the phase ambiguity, M kinds of ambiguities of ϕ_i^0 would be traversed, and M sets of demodulation results of the overlapping waveform $\tilde{x}_i^n(\kappa)$ would be obtained. And then, $\rho_i(\omega)$ would be calculated using the demodulation results, respectively. Finally, the demodulation results corresponding to the maximum $\rho_i(\omega)$ are the desired codes. At this time, due to the phase ambiguity of $\hat{\varphi}_i$, the demodulation result is also ambiguous, but the phase ambiguity can be eliminated in the calculation of $\rho_i(\omega)$ and the initial phase estimation $\hat{\theta}_i$ therefore exists ambiguity.

7 Complexity analysis

Considering the practical implementation of these estimation methods, computational complexities would be analyzed in this section.

The computational complexity is a relatively complicated issue for SVD processing. Generally speaking, time complexity is adopted to reflect the computation cost. For example, for matrix $\mathbf{A}_{m \times n}$, the time complexity could be denoted as $O(n^3)$. In this paper, $n = N = pN_s$ and the complexity could be expressed as $O(N^3)$ correspondingly. What $O(N^3)$ means is that the computational complexity increases exponentially with frame length N. As a result, long frame length would lead to a large computational load, and the methods are more suitable for PCMA signals with shorter frame length. Long frame PCMA signals demand fast SVD methods to ensure the practicability of algorithm.

The main computational complexities of all the modulation parameters after SVD processing are listed in Table 1. To measure complexities of the proposed methods, multiplication and addition operation times are counted. Besides, complex and real operations are not distinguished.

Table 1 Complexities of the proposed schemes

Parameters	Symbol timing phases	Amplitude attenuations	Frequency offsets	Carrier phases
Complexities	$2 \times (11pPH + 3)$	$2 \times (PH + 2)$	$34MPHQ$	$34PH$

Q is the number of the discrete frequencies needing to traverse, and it is determined by the desired frequency resolution and the assumed frequency intervals. Compared to the scheme proposed in [12], the computational complexity of the FOE method in this paper is increased by a factor of M. This is because traversing operation is adopted to filter the fake values out.

It could be observed from the table that the computational complexities are nearly inappreciable by comparison with the SVD processing. So long as the SVD is settled out, the schemes in this paper is practicable and feasible. At the same time, long frame length would lead to significant computational burden, challenging the implementation of the proposed algorithms.

8 Simulation

Simulations were performed using MATLAB 2020a software to verify the effectiveness of the schemes proposed in this paper. The estimation performance was assessed using varying E_s/N_0 (the total energy per modulated symbol of the two mixed signals divided by the power spectral density of the noise) and frame number P (the length of the signal segment used in estimation).

8.1 Symbol timing phase estimation

In the symbol timing phase estimation, QPSK modulation is adopted for both signals, the symbol rate $R_B = 5$ MHz, symbol frame length $N_s = 2092$, sync code length $H = 52$, up-sample times $p = 4$, amplitude attenuations $h_1 = 1.0$, $h_2 = 0.8$. A square root raised cosine filter with a roll-off factor of 0.35 is used in both shaping and matched filters in the two signals with equivalent channel durations $[-4T, 4T]$. ω_i, τ_i, θ_i are randomly selected within their specified ranges, and $\omega_1 \neq \omega_2$, $\tau_1 \neq \tau_2$.

Figure 4 displays the results of the comparison among the cyclic moments (CM)-based method, the polyphases (PP)-based method [10], and the modified method in

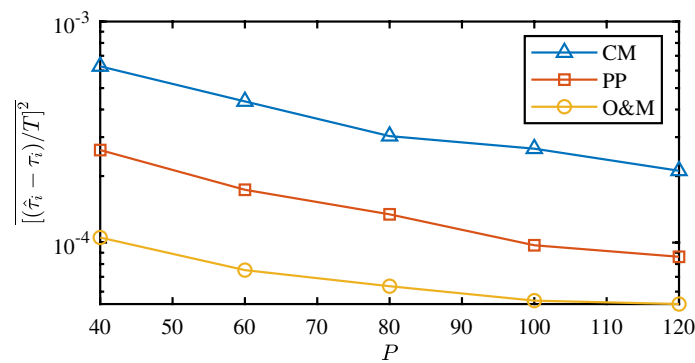**Fig. 4** Performance of different symbol timing estimators versus E_s/N_0, QPSK modulation, $P = 40$

Fig. 5 Performance of different symbol timing estimators versus P, QPSK modulation, $E_s/N_0 = 6$ dB
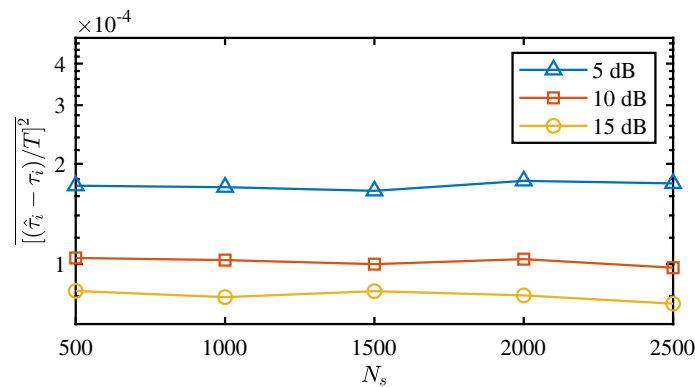

Fig. 6 Performance of different symbol timing estimators versus N_s and E_s/N_0, QPSK modulation, $P = 40$

this paper (O &M). The averaged mean square errors (MSE) of symbol timing phase estimation $\overline{[(\hat{\tau}_i - \tau_i)/T]^2}$ are plotted against E_s/N_0 for a fixed frame number P. It can be observed that the method in this paper, modified O &M, results in the lowest error rates, indicating its superior performance over the other two methods.

In Fig. 5, the performance of different methods is demonstrated for a fixed E_s/N_0 of 6 dB with respect to the frame number P, while the other parameters were kept the same as the ones in Fig. 4.

From Figs. 4 and 5, it can be concluded that the method proposed in this paper shows lower error variance and perform better than the CM-based and PP-based methods.

To further evaluate the robustness and generalizability of the proposed scheme, performance curves under various frame lengths and sync code lengths are provided. Figure 6 shows the averaged MSE of symbol timing phase estimation versus frame length N_s and E_s/N_0. It could be inferred from the figure that frame length has slight impact on the estimation of symbol timing. In other words, the method could be widely applied to PCMA signals with various frame lengths.

Figure 7 shows the estimation performance versus sync code length H and E_s/N_0. It is clearly depicted that the averaged estimation MSE continuously decreases with the increase of H. The essence of the phenomenon is that the increase of sync code length
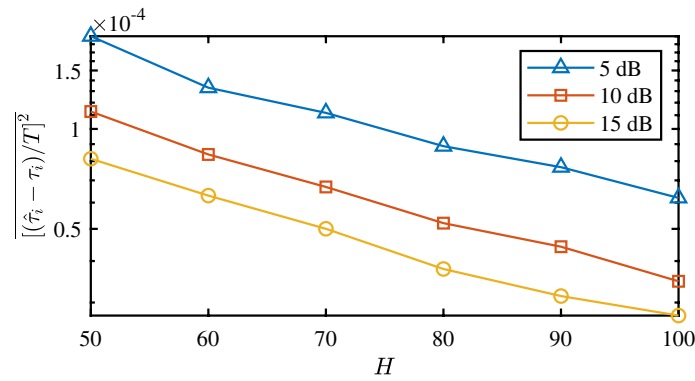
Fig. 7 Performance of different symbol timing estimators versus H and E_s/N_0, QPSK modulation, $P = 40$

H leads to an increment in the volume of aid data. Therefore, the scheme has superior advantage when the PCMA signal owning a long sync code.

The influences of frame length and sync code length are almost the same in the estimation of amplitude attenuation, frequency offset, and carrier phase, as the principle coincides. For simplicity, this paper will not provide the simulation results in turn.

8.2 Amplitude attenuation estimation

As for the amplitude attenuation estimation, BPSK, QPSK, 8PSK, 8QAM, and 16QAM modulations are adopted, respectively, while all other parameters remain the same as those in Fig. 4.

Figure 8 shows the averaged normalized squared amplitude attenuation estimation errors $\overline{[(\hat{h}_i - h_i)/h_i]^2}$ for different modulations versus amplitude ratio h_2/h_1 with a fixed frame number P and E_s/N_0.

Obviously, the estimation errors are high in the low h_2/h_1 ratio regime, where the powers of the weaker signals in PCMA signals are too faint to be estimated. In the high h_2/h_1 ratio regime, or equivalently, when $h_2/h_1 \geq 0.6$, the method shows outstanding performance in amplitude attenuation estimation.

In Fig. 9, we compare our DA-based method with the CM-based method [11]. QPSK modulation is adopted and the parameters are the same as Fig. 8. It is evident from the depicted results that, compared with the CM algorithm, the DA algorithm is more
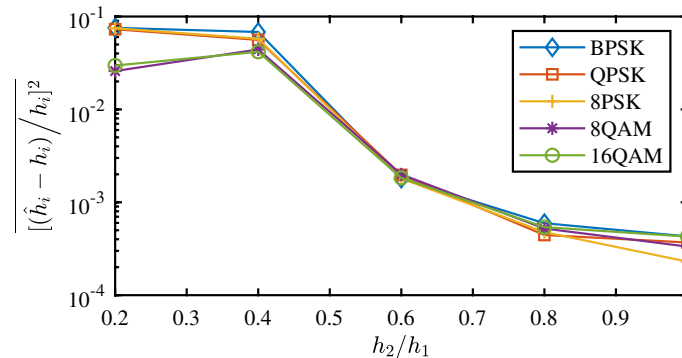

Fig. 8 Performance of amplitude attenuation for different modulations versus h_2/h_1, $P = 100$, $E_s/N_0 = 6$ dB
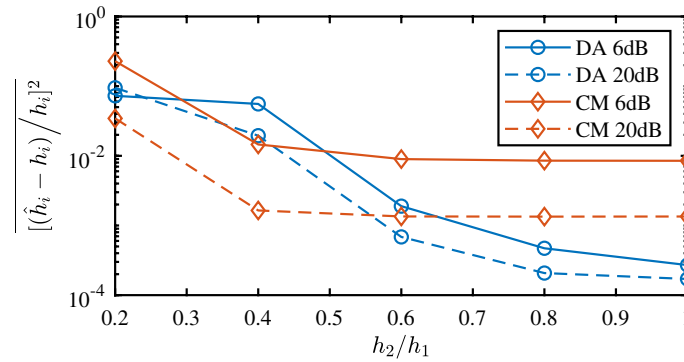
Fig. 9 Performance of different amplitude attenuation estimators versus h_2/h_1, QPSK modulation, $P = 100$

suitable for PCMA signal amplitude attenuation estimation, in particular when the energy of two signals is comparable.

8.3 Frequency offset estimation

When engaged with the frequency offset estimation, 8PSK modulation is adopted, frequency offsets satisfy $|\omega_i| \leq \pi/N_s T$, and all the other parameters are the same in Fig. 4.

Figure 10 shows the MSE of frequency offset estimation $[(\hat{\omega}_i - \omega_i)/(2\pi R_B)]^2$ versus E_s/N_0 with a fixed frame number P. To investigate the performance of the FOE estimation algorithm proposed in this paper, we compare it with the method of *Yang* [12] under the same conditions. *Li* denotes the method proposed in this paper, and *Yang* denotes the method in the paper [12]. It can be observed that at low E_s/N_0, the *Li* method is inferior to the *Yang* method, while the estimation errors decrease with E_s/N_0 and becomes better than the *Yang* method, gradually. This is attributed to the demodulation of the overlapping waveform, more specifically, the bit error rate of overlapping waveform demodulation is high at low E_s/N_0, which has a negative impact on the estimation, and the demodulation results tend to be correct with E_s/N_0 increases; then, the estimation accuracy of the *Li* method improves rapidly, showing lower estimation error than the *Yang* method.
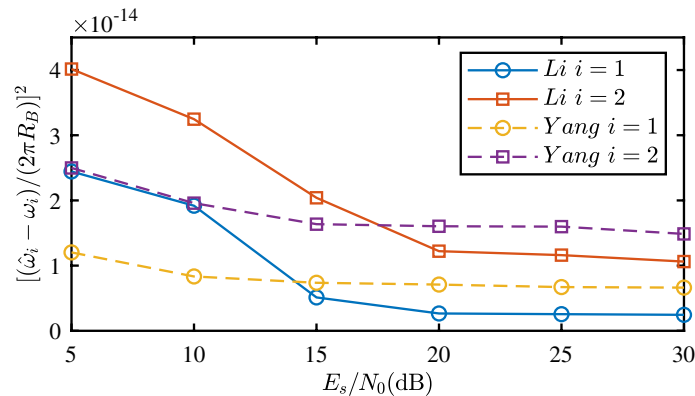

Fig. 10 Performance of different frequency offset estimators versus E_s/N_0, 8PSK modulation, $P = 40$
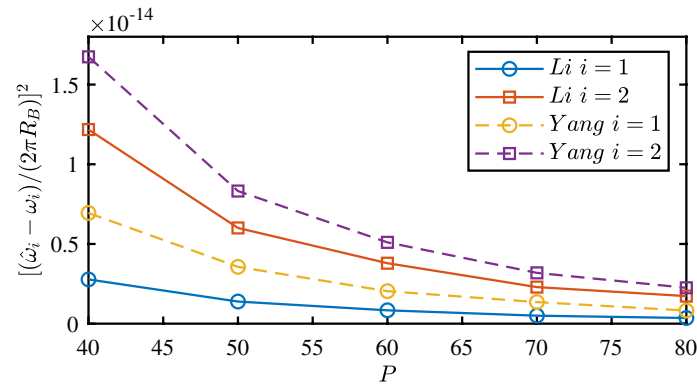
Fig. 11 Performance of different frequency offset estimators versus P, 8PSK modulation, $E_s/N_0 = 20$ dB

From the results depicted in Fig. 11, it is clear that for a fixed E_s/N_0 of 20 dB, when the frame number P increases, the performance of the different methods is improved, indicating that larger frame numbers yield superior performance, and the *Li* method performs better under the given conditions. All the parameters are consistent with those in Fig. 10.

The simulations indicate that if only the accuracy of overlapping waveform demodulation is guaranteed, the algorithm proposed in this paper would be effective for FOE estimation of PCMA signals and outperform the *Yang* method, so that can be used in conjunction with the *Yang* method according to the realities.

8.4 Carrier phase estimation

With respect to the estimation of the initial carrier phase, 8PSK modulation is adopted, and all the other parameters are the same as those in the FOE simulation. In order to evaluate the benefits of the DA-based method proposed in this paper, we compare it with the CM-based method [10].

As shown in Fig. 12, the averaged absolute carrier phase estimation errors $\left|\hat{\theta}_i - \theta_i - m2\pi/M\right|$ of the DA-based and CM-based methods are plotted against E_s/N_0. By the error definition, M-fold ambiguity, which is a common issue in any blind estimation scheme of carrier phase, is eliminated.
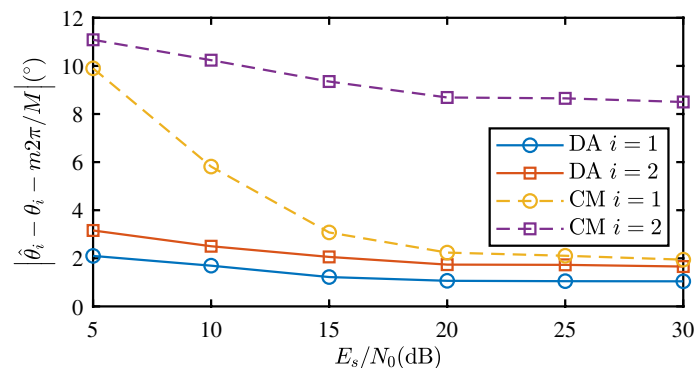

Fig. 12 Performance of different carrier phase estimators versus E_s/N_0, 8PSK modulation, $P = 40$
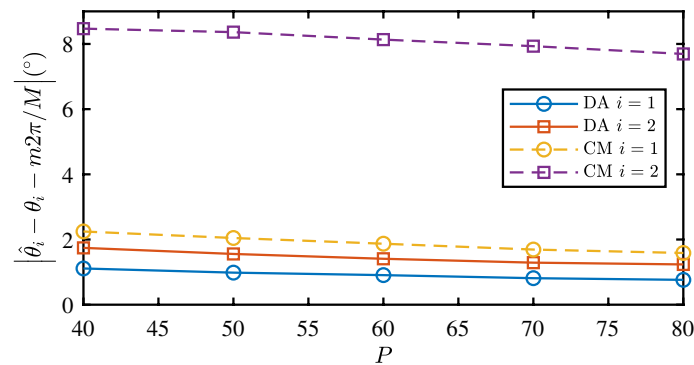
Fig. 13 Performance of different carrier phase estimators versus P, 8PSK modulation, $E_s/N_0 = 20$ dB

In Fig. 13, estimation errors versus frame number P for a changeless E_s/N_0 of 20 dB are depicted.

Apparently, the simulation results show that the DA-based method proposed in this paper yields lower error than the CM-based method under the simulation conditions.

9 Conclusion

In this paper, considering the frame cyclic features, we have presented schemes for the estimation of the symbol timing phase, amplitude attenuation, frequency offset, and carrier phase of APM-modulated PCMA signals (e.g., BPSK, QPSK, 8PSK, 8QAM, 16QAM, etc.) in totally blind condition. More to the point, the schemes are especially effective for high-order APM modulations (e.g., 8PSK). Compared with the algorithm based on cyclic statistics in [9–11] and the ML method proposed in [12], the schemes proposed in this paper yield superior performance, on the advantage of exploiting the sync waveform, overlapping waveform and their demodulation results as aid data. Based on these advantages, this paper has put forward a practicable modulation parameters estimation algorithm with effective performance, which provides an important basis for the blind separation of PCMA signals. Of course, the algorithm is only efficient when the signals are encoded asynchronously. The estimation methods under synchronous encoding conditions still need to be studied. In addition, the overlapping waveform would produce unfavorable effect on the estimation as soon as the signal-to-noise ratio is too low to be demodulated. At this time, sync waveform could be used alone to estimate the modulation parameters.

Abbreviations

PCMA	Paired carrier multiple access
SVD	Singular value decomposition
SIC	Self-interference cancelation
BP	Back propagation
ML	Maximum-likelihood
DA	Data-aided
APM	Amplitude and phase modulation
FOE	Frequency offset estimation
AWGN	Addictive white Gaussian noise
CM	Cyclic moments
PP	Polyphases
MSE	Mean square error

Li *et al. EURASIP Journal on Advances in Signal Processing*   (2023) 2023:95

Page 18 of 18

References
1. M. Dankberg, Paired carrier multiple access (PCMA) for satellite communications, in *17th AIAA International Communications Satellite Systems Conference and Exhibit*, p. 1398 (1998)
2. K. Liu, H. Li, X. Dai, X. Xu, Single channel blind separation of cofrequency MPSK signals, in *Proceedings of the International Conference on Internet, Education and Information Technology*, pp. 42–46 (2006)
3. T. Shilong, Z. Hui, G. Na, Single-channel blind separation of two QPSK signals using per-survivor processing, in *APC-CAS 2008-2008 IEEE Asia Pacific Conference on Circuits and Systems*, pp. 473–476. IEEE (2008)
4. P. Cui, H. Jiang, K. Cao, T. Li, The DFF-PSP iterative separation and theoretical bound for PCMA with long memory. Chin. J. Electron. **25**(5), 880–885 (2016)
5. Y. Yang, H. Peng, D. Zhang, X. Dai, Markov chain Monte Carlo-based separation of paired carrier multiple access signals. IEEE Commun. Lett. **20**(11), 2209–2212 (2016)
6. Q. Deng, S. Zhang, G. Chen, H. Lu, Blind separation of PCMA signals based on iterative quantum genetic optimization, in *2019 International Conference on High Performance Big Data and Intelligent Systems (HPBD &IS)*, pp. 35–40. IEEE (2019)
7. Z. Peng, H. Li, Single-channel blind source separation of two MPSK signals based on stack algorithm, in *2020 International Conference on Wireless Communications and Signal Processing (WCSP)*, pp. 388–393. IEEE (2020)
8. C. Wei, H. Peng, J. Fan, Single-channel demodulation algorithm for non-cooperative PCMA signals based on neural network. KSII Trans. Internet Inf. Syst. (TIIS) **13**(7), 3433–3446 (2019)
9. A. Feder, W. Wicke, M. Hirschbeck, W. Gerstacker, Blind symbol rate and frequency offset estimation for pcma signals via cyclic correlations. In: GLOBECOM 2020-2020 IEEE Global Communications Conference, pp. 1–7 (2020). IEEE
10. A. Feder, W. Gerstacker, M. Hirschbeck, Blind symbol timing and carrier phase estimation for pcma satellite signals via cyclic statistics, in *2021 IEEE Global Communications Conference (GLOBECOM)*, pp. 01–07. IEEE (2021)
11. A. Feder, M. Hirschbeck, W. Gerstacker, Blind estimation of the carrier powers and SNRs in PCMA satellite signals by cyclic statistics, in *MILCOM 2022-2022 IEEE Military Communications Conference (MILCOM)*, pp. 913–919. IEEE (2022)
12. Y. Yang, D. Zhang, H. Peng, Frequency offset estimation of the linear mixture of two co-frequency 8 phase-shift keying modulated signals. IET Signal Proc. **9**(2), 186–192 (2015)
13. M. Waldecker, R. Marsalek, Impact of hardware imperfections and imperfect channel knowledge on SVD-precoded MIMO, in *2022 32nd International Conference Radioelektronika (RADIOELEKTRONIKA)*, pp. 01–04. IEEE (2022)
14. M. Oerder, H. Meyr, Digital filter and square timing recovery. IEEE Trans. Commun. **36**(5), 605–612 (1988)
15. B. Paden, A matched nonlinearity for phase estimation of a PSK-modulated carrier (corresp.). IEEE Trans. Inf. Theory **32**(3), 419–422 (1986)

Publisher's Note
Springer Nature remains neutral with regard to jurisdictional claims in published maps and institutional affiliations.